EWSHM 2024
11th European Workshop on Structural Health Monitoring

Comparison between acoustic emission sensors and piezoelectric patches for damage detection in concrete beams

Gabriele CAZZULANI [1], Haris ALEXAKIS [2]
[1] Politecnico di Milano, Milan, Italy, e-mail: gabriele.cazzulani@polimi.it
[2] Aston University, Birmingham, UK, e-mail: c.alexakis@aston.ac.uk

Abstract. Acoustic emission (AE) sensing is an established technique to monitor crack nucleation and propagation in different types of structural elements and for different damage scenarios. Although effective for crack monitoring in civil infrastructure, off-the-shelf AE sensors can be expensive, discouraging their installation in large numbers for assessing the global structural performance or monitoring multiple assets in the infrastructure network. For this reason, this paper explores the use of piezoelectric (PZT) patches as an alternative low-cost solution to AE sensors. These patches are considerably cheaper, do not require external power supply and can be easily attached to existing structural elements or embedded into new structures. Moreover, thanks to the direct and inverse piezoelectric effect, the same set of patches can act both as sensors and actuators, meaning that they can be used to "passively" monitor crack propagation over time, as well as to locate and characterise damage in ageing structures at a certain time by using the patches as emitters and receivers of waves. In this framework, this paper proposes a comparison between traditional AE sensors and PZT patches. The comparison is performed on a set of three concrete beams subjected to four-point bending loading, each equipped with two grids of sensors, i.e. 8 AE sensors and 8 patches. The beams are tested under increasing monotonic loading, from zero-load uncracked condition up to collapse.

Keywords: non-destructive testing; ultrasonic guided waves; acoustic emission sensing; ageing infrastructure; condition assessment

Introduction

Civil infrastructure deteriorates due to material fatigue, overloading, seismic action, ground movement and environmental effect. This affects the serviceability and structural integrity of civil assets, such as bridges, causing major socio-economic disruptions and life loss [1]. Climate change and energy/resource depletion force transport infrastructure managers to build less, and at the same time guarantee public safety. That requires the transformation of

Media and Publishing Partner
https://doi.org/10.58286/29827

current maintenance and operational decision-making practices to effectively (i) estimate the remaining life of deteriorating assets, (ii) quantify, prioritise and assess the effectiveness of retrofitting interventions, and (iii) restrict, if needed, the traffic loading and speed.

Ageing infrastructure suffers from local deterioration that will not necessarily manifest itself in the material surface or global response [2]. For instance, masonry bridges suffer from localised failures (e.g. arch ring separation/delamination, spandrel-arch barrel separation) that may mobilise, at a later stage, partial or global collapse mechanisms. Internal reinforcement corrosion is the dominant deterioration mode of concrete bridges (e.g. 66% of deteriorating bridges in Japan are found to suffer mostly from chloride ingress, plus 5% from carbonation/alkalinity decrease) [3].

Non-destructive testing (NDT) techniques, such as acoustic emission (AE) sensing and ultrasonic guided waves, are studying the propagation of low-amplitude (~nm), high-frequency (>10kHz) stress waves associated with material defects. AE sensing has been the main 'passive' NDT technology to detect local failures in infrastructure materials, such as leakage detection in high-pressure containers and valves [4] and material degradation in steel and concrete structures [5]. In concrete, high AE wave attenuation has restricted the use of AE PZT sensors to mostly 'local SHM' approaches, focusing on specific structural elements emitting high-energy AE waves (e.g. cables, tendons). Advances in high-sampling rate systems and signal processing allow today wider potential applications in bridge monitoring for: (i) 3D damage localisation (formation of new cracks, existing cracks), (ii) source discrimination (crack characterization; shear, tensile or mixed-mode crack), (iii) damage severity assessment (monitoring of the damage level at regions), (iv) study of corrosion, (v) study of fatigue and creep, and (vi) evaluation of retrofitting interventions (i.e. FRPs) [5].

On the other hand, ultrasonic guided waves is an 'active' NDT technique that has been widely used for defect detection in long steel linear structures, such as rail tracks and pipelines [6], as well as in plate-like structures such as fuselage panels for helicopters and aircrafts [7] and less in the long-term monitoring of ageing masonry and concrete structures, such as bridges. It is based on the use of a grid of sensing/actuating devices, where iteratively one of them acts as actuator, sending a wave in the structure, while the others are configured as sensors, "listening" the wave signal propagating from the actuator. Changes in the structure (such as defects and cracks) cause the formation of discontinuities, which modify the propagation properties, reflecting back part of the energy and refracting the propagating part.

The limitation in the use of this technique for civil structures is mainly related to high dissipation, causing a limited propagation capability of the wave and requiring high power source, and to the complexity of the wave field (presence of different wave modes, non-homogeneity of the material), which makes the interpretation of the result difficult. However, provided that sufficient power source is available, the technique has unique advantages, such as the capability of detecting the current structure condition and not only the evolution of crack propagation from the installation of the monitoring system. Moreover, recent advances in the field of metamaterials and wave propagation control could pave the way to better instruments to guide waves for an imaging of the internal condition of the structure.

In this work, we are studying the use of a low-cost sensing system, with the aim of combining the advantages of AE and guided waves sensing with a unique instrumentation layout for concrete and masonry structures. The system is based on low-cost PZT patches (~$50-100 each) bonded on the structure and connected to a proper electrical circuit for signal conditioning. Thanks to the known piezoelectric material properties, the same patches are used alternatively as sensors and actuators, so that both AE and guided wave sensing can be performed.

The first section that follows describes the monitoring systems and experimental setup used for comparing the techniques. The second section presents results from event

localisation and wave propagation analysis as deflection increases in four-point bending tests of reinforced concrete beams. The low-cost system performs localisation with comparable precision to the AE commercial system, while discontinuities are detectable during the guided wave tests when patches are used as actuators.

1. Experimental setup

1.1 Sensing system

1.1.2 Acoustic Emission sensors

The AE system used in this study comprises an off-the-shelf PCI Express-based 8-channel board offering up to 10 MHz sampling rate per channel. The board acquires signals from eight PZT AE sensors with resonant frequency 55 kHz and operating frequency range 40-100 kHz. Sensors of similar frequency range are commonly reported in literature for assessing the condition of concrete and masonry structures [5]. The sampling rate was set at 1 MHz per channel, which is 10 times larger than the maximum frequency of interest, 100 kHz. All sensors incorporate a 40 dB signal preamplifier.

1.1.3 Piezoelectric patches

The patch-based AE system is based on low-cost D13 piezoelectric patches from Physics Instruments, bonded to the structure through 3M DP460 glue. Each patch is connected to a conditioning circuit for signal amplification and acquired through a National Instruments board (cDAQ modular board with high-speed MI9222 modules) with 500 kHz sampling frequency. In order to compare the results with those from the commercial AE system, signals are band-pass filtered in the range 20-100 kHz.

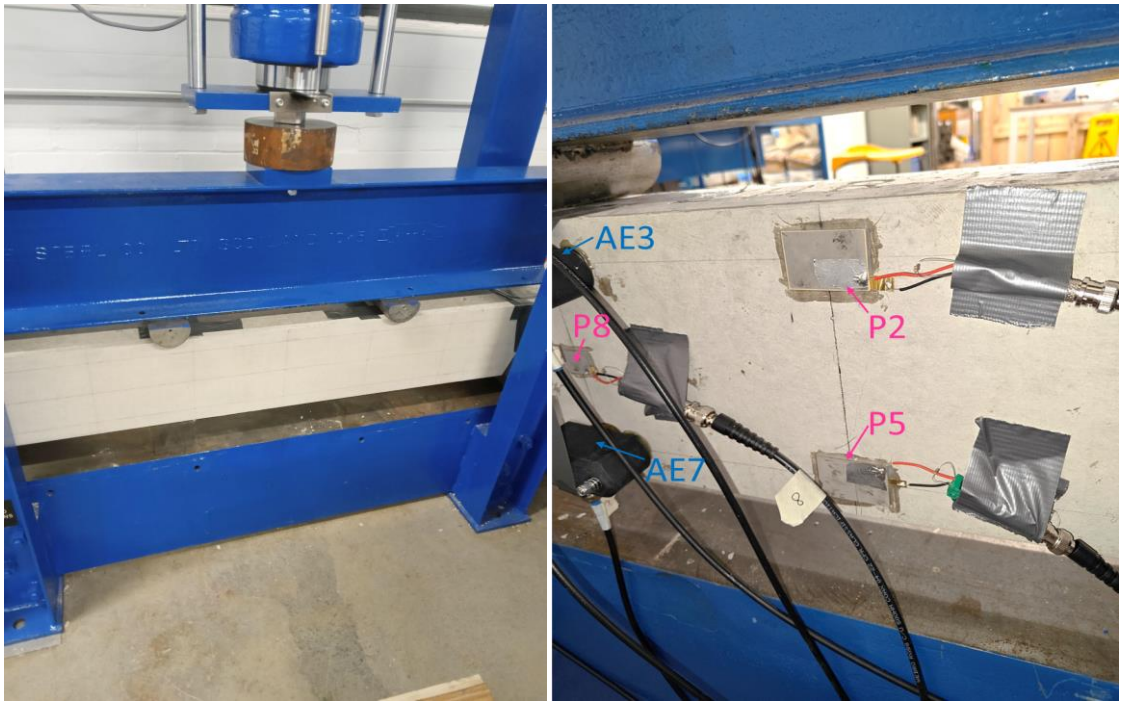

Fig. 1. Left: Front view of the rig and the undeformed specimen. Right: Detail of the back side of the beam with PZT patches and AE sensors (see Fig. 2 for complete numbering of sensors)

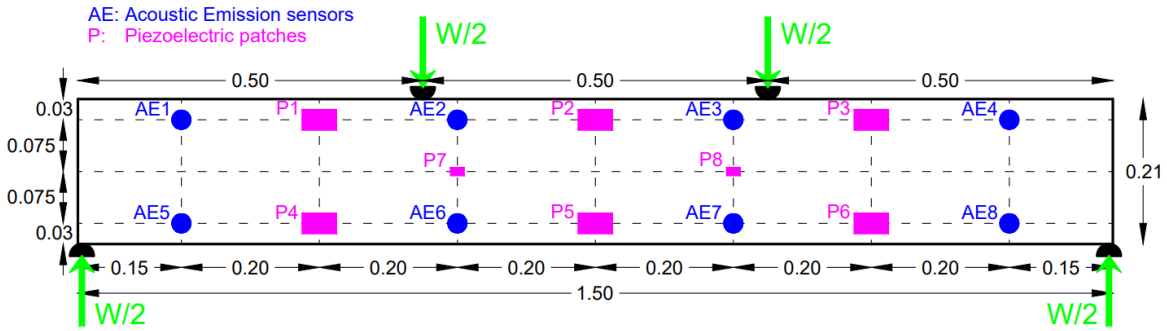

Fig. 2. 'Ghosted' view of the specimen (orientation as in Fig. 1-left) showing the location of the loading points and sensors installed at the back surface. All dimensions are in metres. The dashed lines are reported also on the beam for better visualisation of the cracks location in the following figures

1.2 Specimens and loading

In order to test the combined PZT AE and patches system, three reinforced concrete beams were subjected to monotonic, displacement-controlled, four-point bending tests. Details of the rig, specimen dimensions and location of sensors are shown in Figs 1 and 2.

The three specimens are standard UK reinforced concrete lintels with dimensions 150 x 21 x 14 cm (L x H x W). The longitudinal reinforcement is 1H8 (top) and 2H16 (bottom) bars, and shear reinforcement H8/11cm, with 5cm concrete cover. The concrete is a 40N mix, i.e. designed to achieve a minimum strength of 40 MPa when tested in accordance with BS EN 12390 -2/3.

The test rig is a self-reaction frame with a hydraulic actuator of 400 kN capacity that operates at either force-controlled or displacement-controlled mode. For this study, the latter was selected to enable holding the specimen at different damage levels without inducing further deflection while performing ultrasonic guided waves tests. Between the guided wave tests, the central deflection was increasing at a constant speed of 0.2mm/min to monitor gradual damage. The following table summarises the test protocol:

Table 1. Testing protocol

Central deflection (mm)	Actions
0	Intact specimen. Perform pencil break and guided wave tests
0-3	Impose gradually increasing deflection. AE sensing active with both systems
3	Hold specimen in place. Perform guided wave tests
3-6	Impose gradually increasing deflection. AE sensing active with both systems
6	Hold specimen in place. Perform guided wave tests
6-failure	Impose gradually increasing deflection until failure

Pencil break tests were performed at the top surface of the undeformed specimen, and in particular, 5 breaks per grid line (see Fig. 2) to identify the wave speed propagation. The large diagonals of the grid were considered, and in particular the time lag between AE1 and AE8 when breaking the pencil at the top-left corner of the specimen, and between AE4 and AE5 when breaking the pencil at the top-right corner. Assuming the largest possible distance between sensors minimises deviations due to the heterogeneous properties of concrete, providing a more representative value, which was estimated at 1897 m/s.

Guided wave tests are performed when holding the specimen in place at deflection 0, 3, 6 mm and after failure, as discussed in Table 1. For the first specimen only, guide wave tests were additionally performed at central deflection 0.5, 1 and 1.5 mm to explore the behaviour of the signals at denser deformation levels when cracks are not visible.

During the guided wave tests, each one of the eight patches was used as an actuator while the other AE sensors and patches as sensors. This is repeated 20 times for each test condition for averaging purposes and replicated for all the actuator/frequency combinations. Two different tone bursts, having a central frequency of 60 kHz and 100 kHz respectively have been considered. The choice is a trade-off between the need of reducing the natural attenuation of the wave (which suggests lower frequencies) and the detection capability which suggests higher frequencies in order to have lower wavelength and less superposition between the "main" wave and the reflections from the boundaries.

2. Results

2.1 Damage description and localisation

The damage pattern in all three specimens has been nearly identical. Figs. 3-top and 4-top show the cracks of the second specimen after imposing central deflection 3 mm and 6 mm respectively. The second specimen failed at 6 mm central deflection. In all three specimens, vertical bending cracks start to appear at the bottom fibres at central deflection 1.5 mm. The cracks propagate upwards as deflection increases up to 3 mm, as shown in Fig. 3-top, where the bending cracks are numbered from 1 to 5.

In the second gradual deformation stage (3-6 mm), the main damage activity is concentrated between the top-right loading roller and bottom-right support, resulting in a shear diagonal crack, indicated with the number 6 in Fig. 4-top. Note that in Figs 3-top and 4-top, 15 cm-long segments at both ends of the beam are behind the frame and not shown.

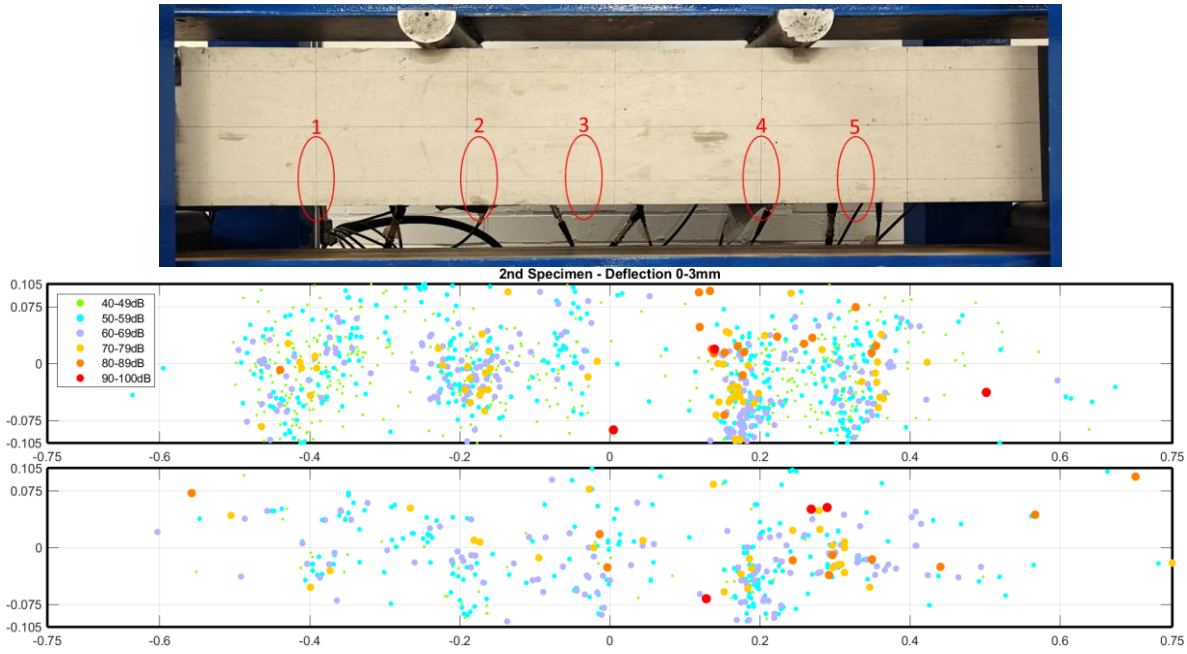

Fig. 3. Damage localisation for 0-3 mm gradual deflection. Top: Front view of second specimen at imposed deflection 3 mm. Centre: AE events localisation derived from the AE system. Bottom: AE events localisation derived from PZT patches

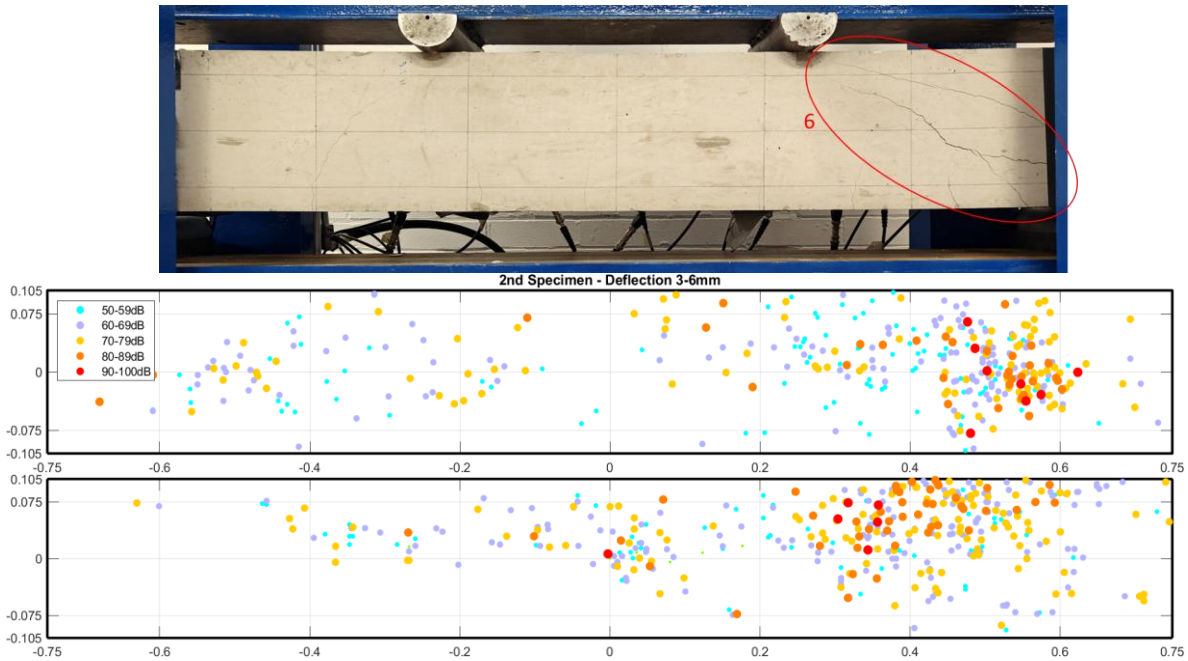

Fig. 4. Damage localisation for 3-6 mm gradual deflection. Top: Front view of second specimen at imposed deflection 6 mm. Centre: AE events localisation derived from the AE system. Bottom: AE events localisation derived from PZT patches

The event localisation mapping shown in Figs. 3 and 4 are derived by considering all eight AE sensors (central figure) and all eight PZT patches (bottom figure) respectively. A 'hit' is defined as the moment when a sensor detects activity that exceeds a predefined value, which was set at 0.01 Volts or 40 dB. Although three sensors identifying a hit from the same event are sufficient for localisation in two dimensions, considering all sensors identifying a hit may minimise the errors in calculating the coordinates of the source via regression analysis. In particular, the algorithm first identifies the time differences of sensors hits,

$$\Delta t_i = t_i - t_1 \tag{1}$$

where t_1 is the time of the hit of the reference sensor 1, and t_i of the ith sensor. Subsequently, the time differences are calculated by assuming values for the coordinates of the source x_s, y_s, based on the following expression,

$$\Delta t_{i,s} = \left[\sqrt{(x_i - x_s)^2 - (y_i - y_s)^2} - \sqrt{(x_1 - x_s)^2 - (y_1 - y_s)^2}\right]/v \tag{2}$$

where x_1, y_1 are the coordinates of the reference sensor 1, x_i, y_i of the ith sensor, and v is the wave propagation speed. The regression analysis proceeds by estimating the source coordinates that minimise the quantity,

$$\chi^2 = \sum\left(\Delta t_i - \Delta t_{i,s}\right)^2 \tag{3}$$

The event localisation mapping shown in Figs. 3-centre and 4-centre is in excellent agreement with the observed cracks at the gradual deflection stages 0-3 mm and 3-6 mm, respectively. The events are grouped with different colours and size of dots based on their amplitudes in the dB scale. Note that the AE data acquisition threshold was set at 40 dB in the first gradual deflection stage, and at 5 0dB in the second stage to optimise data logging due to the increased damage activity. This explains the absence of 40-49 dB dots in Fig. 4-centre, which would otherwise have been more dispersed and frequent compared to the first gradual deflection stage.

Localisation with PZT patches is performed considering the same approach, with the only difference of shifting down the amplitude-dB scale of the plots by 10 units (i.e. the 90-100 dB red dots in the AE sensors plots correspond to 80-90 dB in the PZT patches plots, and so forth), due to a different sensitivity of the two systems.

Apart from the fact that the localisation mapping is denser in the case of the commercial AE system, both AE and patches sensors successfully locate all five bending cracks with n. 1-5, and the large diagonal shear crack with n. 6 on the top-right side of the beam.

2.2 Damage assessment based on wave velocities

Fig. 5 shows the front view of the first specimen at central deflection 6 mm (top) and 7.75 mm (bottom). The cracking pattern is nearly identical to the second specimen. The first specimen first developed vertical bending cracks at symmetric locations, and the total collapse occurred with the large diagonal shear crack shown on the right hand side in Fig. 5-bottom.

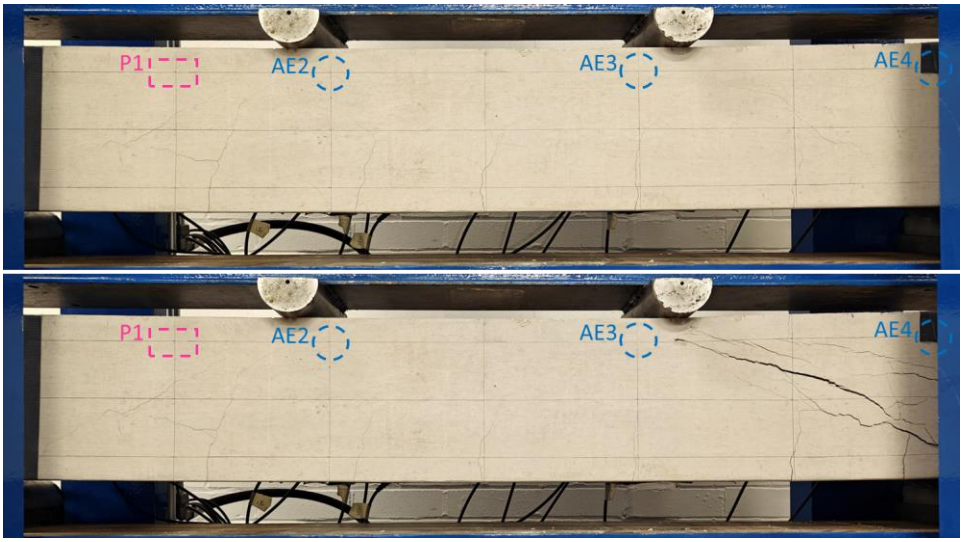

Fig. 5. Front view of specimen 1 at central deflection 6 mm (top) and 7.75 mm (bottom) indicating with dashed line the location of PZT patch 1 and AE sensors 2, 3 and 4 used in the analysis of Fig. 6.

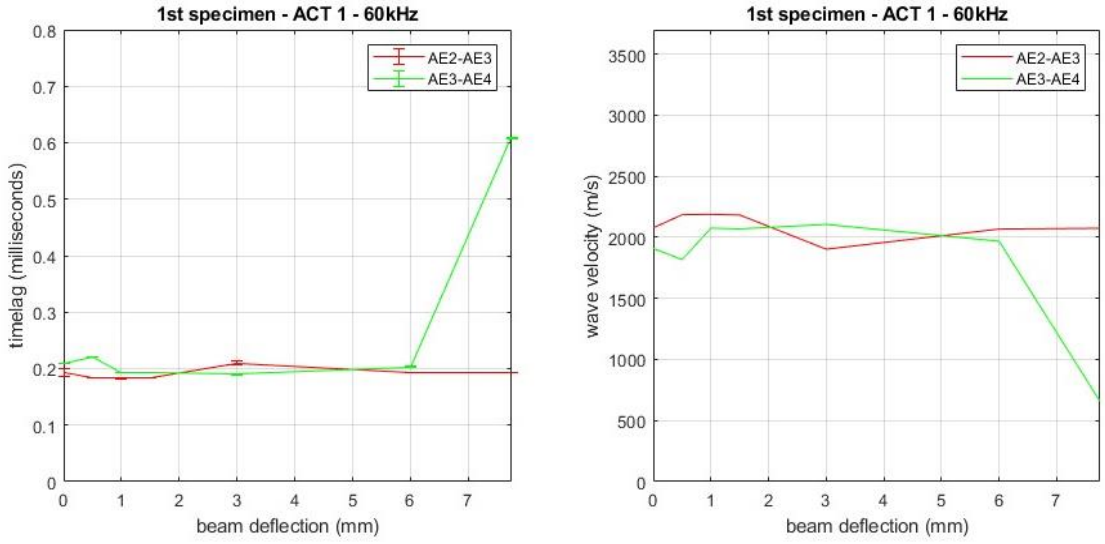

Fig. 6. Guide wave tests with patch P1 selected as the actuator sending 60 kHz pulses, and AE sensors acting as receivers, when holding the first specimen at central deflection 0, 0.5, 1, 1.5, 3, 6 and 7.75 mm. Time lag (left) and wave propagation velocities (right) between AE2-AE3 and AE3-AE4

Fig. 6 presents results of time lag (left) and wave velocity variations (right) during the guided wave tests when holding the specimen at central deflection 0, 0.5, 1, 1.5, 3, 6 and 7.75 mm. In this analysis, we combine the two systems and use PZT patch 1 as actuator, while observing the activity of AE sensors 2, 3 and 4. The choice of the actuator and AE sensors for this example is deliberate as they are all aligned, and contain both a healthy region (i.e. compression zone between AE2-3 that develops no cracking throughout the test) and a damaged region (i.e. area between AE3-4 developing shear crack at the final stage).

In Fig. 6, PZT patch 1 emits ten 60 kHz pulses and the arrival time is recorded by the AE sensors. The average values and standard deviation of the time lag between AE2-3 and AE3-4 are shown in Fig. 6-left. The time lag remains constant in both regions until 6 mm deflection. The presence of the shear crack before deflection 7.75 mm significantly influences the time lag between AE3-4 from 0.2 to 0.6 microseconds. Similarly, the wave propagation velocity remains constant at around 2000 m/s up to 6 mm deflection, while it reduces more than half with the presence of the shear crack. Hence the presence of the shear discontinuity is evident and easily distinguishable by following the suggested approach. This is particularly critical for identifying the presence of internal defects in concrete that do not necessarily manifest on the material surface.

3. Conclusions

The performance of low-cost PZT patches (~$50-100 each) supported with an in-house data logging system to localise and assess damage in reinforced concrete has been compared with commercial AE sensors (~$1,500-2,000 each) supported with a high-performance data logging system. The in-house PZT patches system was able to perform damage localisation comparable to the AE system. Furthermore, the benefit of performing guided wave analysis with a grid of actuators and passive sensors to detect discontinuities that emerge as change in the wave propagation velocity has been also demonstrated.

Acknowledgements

The research was funded by the Royal Society Exchange Grant IES/R2/222240.

References

[1] Deng L., Wang W., Yu Y. (2015) State-of-the-art review on the causes and mechanisms of bridge collapse *ASCE J. Perfor. Constr. Facil.* 04015005
[2] Alexakis, H., Cocking, S., Tziavos, N. I., Din-Houn Lau, F., Schooling, J. & DeJong, M. (2023) 'Sensor-based structural assessment of aging bridges', In Noori, M., Rainieri, C., Domaneschi, M. & Sarhosis, V. (eds.) Data Driven Methods for Civil Structural Health Monitoring and Resilience: Latest Developments and Applications. CRC Press, pp. 76-97
[3] Mutsuyoshi H. (2001) Present situation of durability of post-tensioned PC bridges in Japan, Bulletin-Fib
[4] Mostafapour A., Davoudi S. (2013) Analysis of leakage in high pressure pipe using acoustic emission method, *Applied Acoustics*, 335-342
[5] Behnia A., Chai H.K., Shiotani T. (2014) *Construction and Building Materials*, 65, 282-302
[6] Loveday P.W. & Long C.S. (2022) 'Numerical Analysis of Guided Wave Transmission Through a Long Defect in a Rail Track', *Journal of Nondestructive Evaluation, Diagnostics and Prognostics of Engineering Systems*, 5(4)
[7] Panagiotopoulou V., Sbarufatti C. & Giglio M. (2024) 'SAMAS 2: Structural health and ballistic impact monitoring and prognosis on a military helicopter', *Procedia Structural Integrity*, 54, 482–489